Unmanned Aerial Vehicles Following Photography Path Planning Technology Based on Kinematic and Adaptive Models

Sa Xiao
Department of Public Information, Zibo Vocational Institute, Zibo 255300, China

***Abstract*—As a representative invention of modern intelligent technology, unmanned aerial vehicles are receiving more and more attention in various fields. However, unmanned aerial vehicles cannot autonomously track path planning based on dynamic changes in conventional path planning. To address the aforementioned issues, this study proposes a path-planning algorithm for unmanned aerial vehicles following photography based on kinematic and adaptive models. A global coordinate system and an aircraft coordinate system are constructed based on the motion relationship between the unmanned aerial vehicles and the tracking target, and the two are converted into a horizontal projection coordinate system to digitize the observed data. On this basis, an adaptive control model is established based on the circular tracking path planning algorithm, and finally, simulation experiments and practical application tests are conducted in combination with the unmanned aerial vehicles following and shooting planning algorithm. The results showed that the best fitness of the proposed algorithm compared with the other two algorithms was 97.56, 93.87, and 92.79, and the path time and average speed of the studied algorithm were 38s and 3.4m/s, which were better than the other two algorithms. In the real machine experiment, there were six circular paths planned by the research algorithm, and the relative distance between the unmanned aerial vehicles and the target was within the range of 200m-600m. The actual trajectory had a high degree of overlap with the model planned trajectory. Research has shown that the proposed algorithm not only stabilizes the illumination angle within an effective range in path planning, but also has high convergence and superior path planning performance in practical applications.**

***Keywords*—Kinematic model; adaptive control; unmanned aerial vehicles; path planning; follow photography**

I. Introduction

A. Research Background

With the continuous development of unmanned aerial vehicles (UAVs) and related industries, the application of UAV functions such as aerial target tracking, aerial broadcasting, and aerial photography in military and civilian fields is becoming increasingly broad [1]. In agriculture, UAVs can perform pesticide and fertilizer spraying, real-time monitoring, etc. [2]. In terms of field rescue, UAVs can replace manual entry into the disaster area to take photos and analyze the disaster and casualties based on the images [3]. In military terms, UAVs can perform more extreme reconnaissance, tracking, and target monitoring tasks [4].

B. Research Status

The operation of traditional UAVs requires flight operators and task operators to perform flight tasks and real-time monitoring tasks separately, which reduces the operational difficulty of operators compared to manned aircraft. However, when UAVs perform specific tasks, the monitoring effect on targets is largely influenced by operators, so it is necessary to enhance the optimization of UAV's Tracking Path Planning (TPP) algorithm for targets [5-6]. Many scholars have conducted in-depth research on the intelligent path planning problem of UAVs, mostly based on the combination of improved swarm optimization algorithms and path planning algorithms. Although the improved algorithm can accelerate convergence speed and compensate for the shortcomings of being prone to local optima, it cannot spontaneously re-plan the tracking path based on dynamic changes when tracking target motion changes. Moreover, it is impossible to guarantee the stability of UAV monitoring and illumination angles during flight [7-9].

C. Research Purpose and Innovation

Based on this background, in order to improve the performance of unmanned aerial vehicle tracking and photography path planning (UAV-T3P), achieve automated control, adapt to real-time data changes, and meet dynamic shooting requirements. Innovatively combining kinematic models with adaptive models based on circular tracking path planning algorithm (CTPPA), building experimental models to verify algorithm performance, and finally verifying the feasibility of the algorithm through simulation performance testing and practical applications.

D. Article Structure

The research content is divided into five sections. Introduction is given in Section I Section II is a review of relevant research findings. Section III are the design, simulation experiment analysis, and actual performance verification of the UAV-T3P algorithm based on kinematic and adaptive models. Results and discussion is given in Section IV and finally, the paper is concludes in Section V.

II. Related Works

Adaptive Control Systems (ACS) and kinematic models are often used in the development of intelligent mechanical systems. Bottrell et al. believed that kinematic data can provide a supplementary basis for identifying merging remnants in galaxy evolution, and distinguished the theoretical utility of

merging remnants from other galaxies by analyzing their morphology and kinematic characteristics. They used heterogeneous galaxy clusters and idealized composite images from TNG100 cosmological fluid dynamics simulations, as well as line of sight stellar velocity maps, to calibrate and evaluate the depth classification model. Compared to individual imaging, the combination of imaging and stellar kinematics had a slight improvement in integrity [10]. Li J et al. proposed a Current Sensorless Control Scheme (CSCS) for single-phase uninterruptible power supply inverters under nonlinear loads. By incorporating an adaptive model control method, the load current information was obtained. In the case where the load current was a periodic ideal current, Fourier series simulation of unknown disturbances in the load current was carried out. Moreover, comparative experiments were conducted without the use of current sensors to verify the effectiveness of the adaptive control method in CSCSs [11]. Pang N et al. established a disturbance observer using a neural network when studying the adaptive tracking problem of a class of uncertain nonlinear systems. They utilized a switching threshold triggering mechanism and combined it with backstepping technology to design an adaptive tracking controller. The tracking error converged at an adjustable origin and the closed-loop signal was semi-globally bounded [12]. Yang Y et al. designed a filter-based adaptive control method for under-actuated crane systems with unknown system parameters and nonlinearity. The filter was directly applied to the crane system, causing the system to exhibit nonlinearity during reverse thrust. Then, by using the variable transformation method to reduce the errors of swing angle and position, this scheme has been proven to effectively reduce the tracking error of under-actuated crane systems and converge to any radius [13].

UAVs are increasingly being used in various applications, and their scope of tasks is also expanding [14-16]. Saeed RA et al. discussed the impact of different intelligent algorithms on UAV path planning in complex geographic environments for UAVs. Based on this, a model for improving the optimal path of UAVs with dependent populations was proposed, and performance tests were conducted in different dimensional environments using an improved ant colony optimization algorithm. Evolutionary algorithms could improve convergence speed and further optimize path planning models [17]. Cao Y et al. believed that UAVs are an ideal carrier for sensors and propose a UAV formation path coverage algorithm for aerial photography. This algorithm improved through path coverage and formation control, optimizing the drawbacks of high repetition rate and multiple turns in traditional Probability Road Map (PRM) algorithms. After conducting multiple sets of simulation tests, it has been proven that the algorithm can achieve centralized coverage of aerial photography [18]. Shen K et al. believed that path crossing may lead to UAV collisions during multi UAV flight missions. To address this issue, two collision avoidance Path Planning Algorithms (PPA), namely Separation and Turning, were proposed. This algorithm separated large UAV tasks into multiple small tasks, and multiple UAVs were grouped to fly along the optimized path. Using the proposed algorithm to detect and eliminate potential collision points during flight, the final profit model evaluation showed that the algorithm had superior coverage performance [19]. Puente Castro A et al. proposed the development of a reinforcement learning-based system to calculate the optimal flight path of a UAV group for the calculation problem of multiple optimal planning paths. This method achieved full coverage of path leap regions by repeatedly experimenting and learning self-adjustment models. Due to the limitations of UAV group flight time and map size, using the same control method was more conducive to the execution of field exploration tasks [20]. Finally, the research summarizes the research methods, research results and limitations of the above literature review, as shown in Table I.

TABLE I. LITERATURE SUMMARY TABLE

Authors	Year	Algorithms / Methods Used	Key Results	Limitations
Bottrell C et al. [10]	2022	The morphological and kinematic characteristics of merging relics in distinguishing galaxy merging relics	Combining imaging and stellar kinematics offers a small boost in completeness	The practicality of stellar kinematic data is limited
Li J et al. [11]	2022	A current sensorless control scheme for single-phase uninterruptible power supply inverters under nonlinear loads.	The stability and effectiveness of the system were rigorously analyzed using the Lyapunov method	Suitable for the field of current sensors
Pang N et al. [12]	2022	An adaptive tracking system for uncertain nonlinear systems is designed.	The tracking error is converged and the effectiveness of the method is proved.	The feasibility in UAV system is not verified.
Yang Y et al. [13]	2022	An adaptive control method based on filter is designed.	The tracking error of the driving crane system is significantly reduced.	Suitable for driving crane system control
Saeed R A et al. [17]	2022	A model for improving the trajectory of UAVs dependent on swarm intelligence is proposed.	The algorithm achieves fast convergence and speeds up the path planning process.	The adaptive performance needs to be improved.
Cao Y et al. [18]	2022	Concentrated Coverage Algorithm for UAV Formations Used in Aerial Photography	The algorithm proposed in the paper can achieve centralized coverage of aerial photography	The proposed algorithm has not been tested in the actual scene.
Shen K et al. [19]	2022	DETACH and STEER two collision avoidance path planning algorithms	STEER covers 40% more waypoints than DETACH and generates 20% more profit.	The research sample is limited.
Puente-Castro A et al. [20]	2022	UAV path planning based on reinforcement learning system	It is optimal to establish a single control for each UAV in the cluster.	The flight time of drones is greatly affected by the size of the map

As shown in Table I, although many scholars have made relevant research on kinematic model, adaptive model and UAV-T3P, most of the research on UAV-T3P has not solved the problem that UAV can autonomously plan the path after tracking the dynamic changes of the target, and the kinematic model, adaptive model and UAV-T3P have not been combined at this stage. Therefore, this study constructs the UAV-T3P algorithm based on kinematic and adaptive models, aiming to improve the UAV's aerodynamic capability by combining ACS, and achieve the expected goal of independently completing ground target tracking and monitoring tasks.

III. Design of UAV-T3P Algorithm based on Kinematic and Adaptive Models

This study first establishes a kinematic model of UAV and tracking target, and digitizes the model to better describe and calculate the relationship between the two. Then, CTPPA combined with ACS modeling is used to meet the real-time monitoring requirements of UAV and tracking targets, and finally, combined with UAV-T3P, the Circular Path (CP) switching in the dynamic process is completed.

A. Kinematic Modeling of UAV Tracking Targets

UVA generally consists of six parts: aircraft frame, Flight Control System (FCS), propulsion system, imaging equipment, remote control, and signal receiver. The FCS exists inside the UVA fuselage, and the remote control and signal receiver are independent of the fuselage. The structure of the UVA fuselage is Fig. 1.

In Fig. 1, the UVA outer fuselage structure includes the fuselage, influencing equipment, FCS, and landing gear. To better describe the motion relationship between UAV and tracking targets, it is preferred to construct a Global Coordinate System (GCS) and an Aircraft Coordinate System (ACS), as shown in Fig. 2.

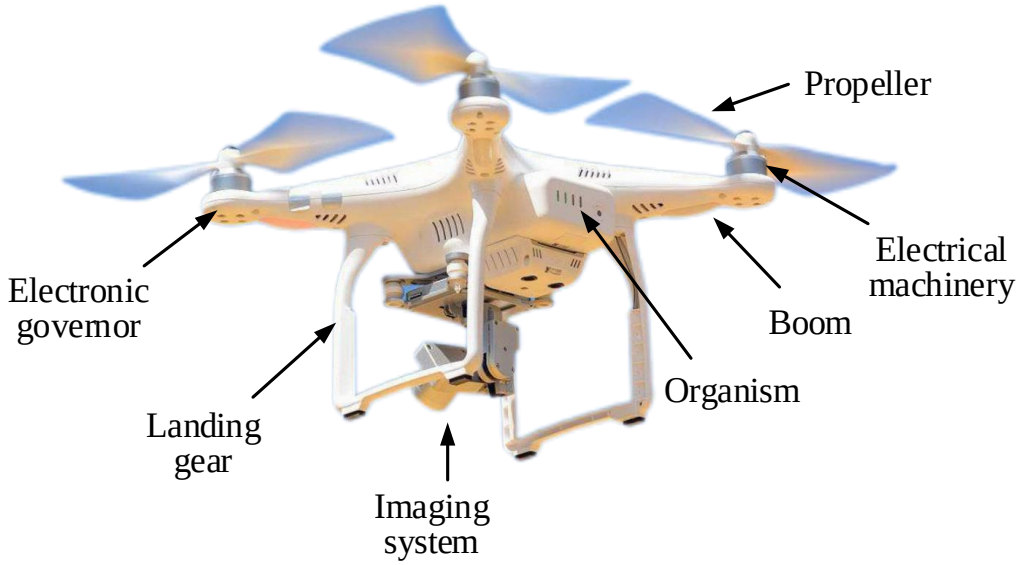

Fig. 1. Schematic diagram of UVA.

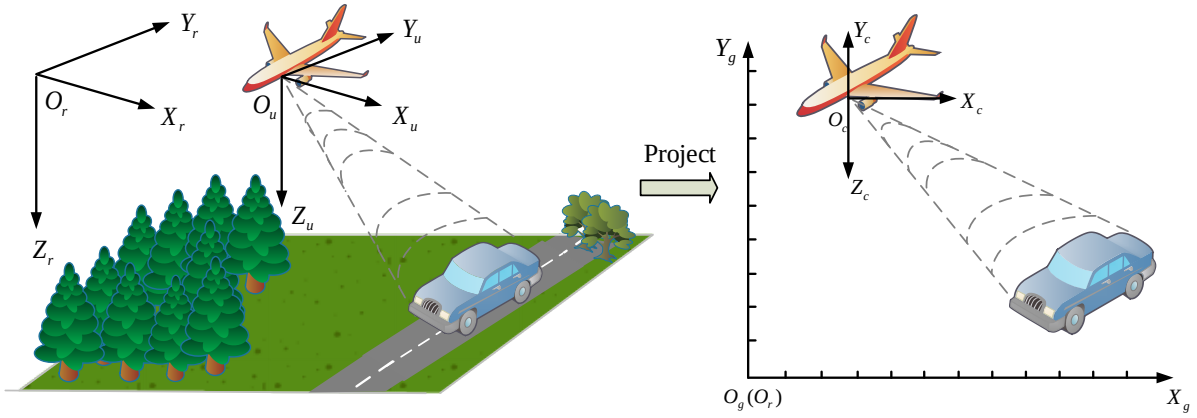

(a) Global coordinate system and aircraft coordinate system for UAV motion

(b) Horizontal projection coordinate system for UAV movement

Fig. 2. Schematic diagram of GCS, ACS, and HPCS.

Fig. 2(a) represents GCS and ACS, while Fig. 2(b) represents the Horizontal Projection Coordinate System (HPCS) that ignores the motion in the Z_r -axis direction in GCS. O_r is the origin of the GCS, fixed at the starting position of the UAV, and Y_r, X_r, Z_r are the three coordinate axes of the GCS, representing the geographical position of due east, due north, and the vertical downward direction of the UAV. O_u is ACS, whose origin is fixed at the geometric center of the UAV connection axis and the stable platform. Y_u, X_u, Z_u are the three coordinate axes of ACS, which are collinear with the vectors of the three coordinate axes of GCS. In Fig. 2(b), O_g represents the origin of HPCS. The origin O_c of the UAV camera coordinate system is a point on the optical axis inside the laser rangefinder. The positive direction of X_c points to the right of the image and is perpendicular to Z_c. The positive Y_c direction points towards the bottom of the image and is perpendicular to the coordinate system plane. Since the UAV is aware of its own motion, the ACS can complete the GCS transformation through translation, and the global coordinates are shown in Eq. (1).

$$(x_r, y_r, z_r) = (x_u, y_u, z_u) + (\Delta x, \Delta y, \Delta z) \quad (1)$$

In Eq. (1), (x_r, y_r, z_r) represents the global coordinates, (x_u, y_u, z_u) represents the aircraft coordinates, and $\Delta x, \Delta y, \Delta z$ represents the displacements on the three coordinate axes affected by UAV motion. Given that the UAV maintains a constant altitude during flight, then $\Delta z = 0$. Although the UAV's own motion may be affected by the aircraft control system and generate errors, resetting ACS to GCS at the end of the tracking cycle can clear the errors. Due to the overlap between HPCS and GCS, the horizontal projection coordinates obtained from the horizontal projection of GCS are expressed in Eq. (2).

$$(x_g, y_g) = (x_r, y_r) \quad (2)$$

In Eq. (2), (x_g, y_g) is the coordinates after horizontal projection. To meet the subsequent modeling requirements, it is necessary to measure the projection of the slant distance Between the UAV and the Tracking Target (B-UAV/TT) on HPCS $X_g O_g Y_g$, as well as the angle Between the UAV and the Tracking Target Line (B-UAV/TTL) and due north, as shown in Eq. (3).

$$\begin{cases} l = \sqrt{(x_{gt} - x_{og})^2 + (y_{gt} - y_{og})^2} \\ \theta = \arctan \dfrac{x_{gt} - x_{og}}{y_{gt} - y_{og}} \end{cases} \quad (3)$$

In Eq. (3), θ represents the angle B-UAV/TTL and the Y_g -axis. l represents the distance B-UAV/TT. x_{gt} and y_{gt} represent the horizontal projection coordinates obtained by converting the tracking target. x_{og} and y_{og} are the coordinates after converting the origin of the camera coordinate system. After the conversion is completed, a kinematic model of UAV and tracking target is built on HPCS, and the UAV kinematic model is Eq. (4).

$$\begin{cases} x_g = v \cdot \sin\psi \\ y_g = v \cdot \cos\psi \\ \psi = u \end{cases} \quad (4)$$

In Eq. (4), x_g and y_g are the horizontal and vertical coordinates of the UAV in HPCS. v represents the speed of the UAV. ψ represents the heading angle. u represents the control variable, which is influenced by real physical factors and has certain limitations, so $u_{\min} \le u \le u_{\max}$. $u_{\min}$ is the minimum velocity of the UAV heading angle, and $u_{\max}$ is the maximum velocity. According to the constant speed and altitude characteristics of UAVs during flight, the heading angle becomes the only variable controlling UAV motion. The kinematic model for tracking the target is Eq. (5).

$$\begin{cases} x_t = v_t \cdot \sin\psi_t \\ y_t = v_t \cdot \cos\psi_t \\ \psi_t = \omega_t \end{cases} \quad (5)$$

In Eq. (5), v_t and ω_t represent the speed of tracking the target and the speed of turning angle, respectively. ψ_t represents the angle between the tracking target's direction of motion and due north.

B. Building an Adaptive Model Based on CTPPA

ACS is a control system that can adapt to dynamic changes in the controlled object by automatically adjusting the control parameters in the system. This study proposes an ACS model based on CTPPA, namely ACS-CTPPA, which can monitor the motion of targets in real-time and plan the optimal path to adapt to changes in target motion. In order for the UAV to continuously track the target, its speed must be greater than the target's speed, and the UAV needs to maintain a certain Relative Distance (RD) from the target. The best motion path that can simultaneously satisfy these two conditions is a CP. Assuming the target is in a stationary state, the UAV performs a CP on one

side of the target while monitoring and illuminating the target in real-time. The state is Fig. 3.

Fig. 3(a) shows the relationship between UVA and the target when the target is stationary, and Fig. 3(b) is the relationship between the center of the circle and the target when UVA moves along a CP. v_{ut} is the tangential velocity component, and v_{un} represents the normal velocity component. When the target is stationary, the RD between the UAV and the aim is mainly affected by the tangential velocity component, and the relative angle is mainly affected by the normal velocity component. In this case, l' and θ' are calculated as Eq. (6).

$$\begin{cases} l' = v_{ut} = v \cdot \sin(\theta - \psi - \dfrac{\pi}{2}) = -v\cos(\theta - \psi) \\ \theta' = \alpha + \beta = \pi - \gamma + \beta = \beta - \gamma \end{cases} \tag{6}$$

In Eq. (6), α and β are the angle between the line connecting the UAV and the center of the CP and the due north direction or the UAV and the target. γ represents the angle between the UAV at the center of the CP and the line connecting the center of the circle and the due north direction. ACS-CTPPA is Eq. (7).

$$\begin{cases} l_m = -v \cdot \cos(\theta - \psi) \\ \theta_m = \beta - \gamma \end{cases} \tag{7}$$

In Eq. (7), l_m and θ_m are the models of the distance and angle B-UAV/TT, respectively. However, considering the existence of errors in actual motion, the variation of the distance and angle B-UAV/TT in practice is Eq. (8).

$$\begin{cases} l_p = l_m + l_d \\ \theta_p = \theta_m + \theta_d \end{cases} \tag{8}$$

In Eq. (8), l_p represents the distance affected by the target motion in practice. θ_p represents the angle affected by the target motion in practice. l_d and θ_d respectively represent the length interference from the motion vector on the extension line and the angle interference from the motion vector perpendicular to the extension line. The error between l and θ is represented by Eq. (9).

$$\begin{cases} e_l = l_p - l_m \\ e_\theta = \theta_p - \theta_m \end{cases} \tag{9}$$

In Eq. (9), e_l and e_θ are the generalized errors of RD and relative angle. In actual tasks, the known variables are l_p and θ_p, and the direction and speed of target movement are unknown. When the change in target motion reaches the standard, it is necessary to plan a new path to adapt to the change in target motion. The rate of change of the center of a CP $O(k)$ is Eq. (10).

$$O(k) = (l_p \cdot \sin\theta, l_p \cdot \cos\theta_p) - (l_m \cdot \sin\theta_m, l_m \cdot \cos\theta_m) \tag{10}$$

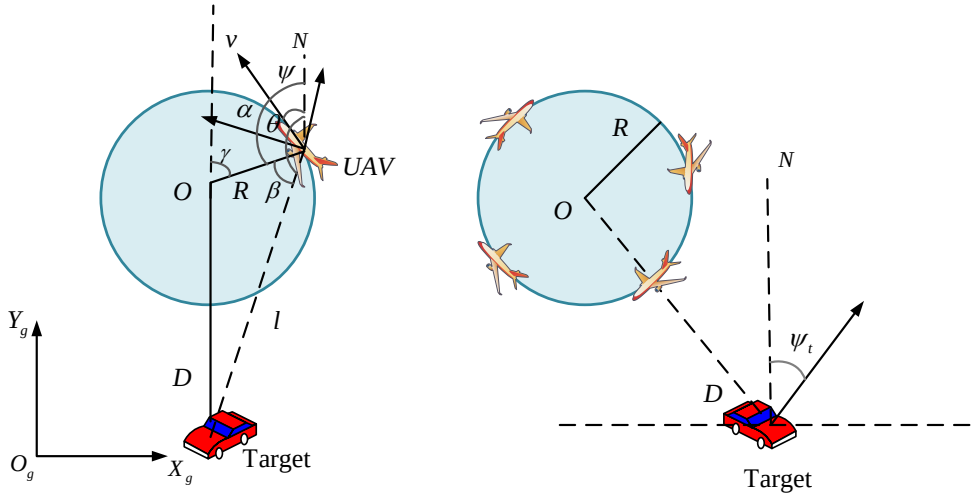

(a) The relationship between UVA and target when the target is stationary

(b) The relationship between the center of the circle and the target during UVA circular path motion

Fig. 3. Definition of UAV and target related variables.

In Eq. (10), tracking the target requires determining the position of the center of the circle in HPCS based on its own position. In Fig. 3(b), O is the center of the CP, R means the radius of the CP, D is the distance from the center to the target, and ψ_t is the angle between the target's direction of motion and due north. Due to the current target position remaining stationary, $R_{\min} \le R \le \dfrac{D_{\max} - D_{\min}}{2}$. The center coordinates of the new CP O' are expressed in Eq. (11).

$$O' = P_t + (-D \cdot \sin\psi_t, D \cdot \cos\psi_t) \tag{11}$$

In Eq. (11), P_t represents the target position. The position of O' will not immediately enter a new path with the movement of the UAV. Small scale movements may lead to the planning of many new circular tracking paths, but each new path will not be switched before reaching the switching point.

C. UAV-T3P Based on Kinematic and Adaptive Models

This study plans a transition route from the current path to the new CP, with the center of the new CP already determined, and designs a UAV-T3P that combines ACS-CTPPA, namely ACS-FP-CTPPA. This study focuses on tracking problems, with UAVs and tracking targets as the main objects. Assuming that the UAV's flight speed and altitude are constant, ignoring the UAV's transition from turning to horizontal flight and environmental factors, only considering the heading angle issue, the path switching planning is Fig. 4.

In Fig. 4, O_1 represents the CP currently being carried out by the UAV, and O_2 represents the new path calculated through ACS-CTPPA that meets the UAV's motion requirements. Point A is the current CP point, and point D is the entry point for the new CP. B is the starting point of the UAV's transition from a turning state to horizontal flight during the transfer path, while C is the endpoint. ψ_s represents the heading angle at the starting point of segment AB when the UAV cuts out, ψ_e represents the heading angle at the ending point of segment AB, and $\psi(t_1)$ and $\psi(t_2)$ represent the heading angles when cutting out t_1 and t_2 on segment CD. When the UAV hovers to point A, the step response through the heading channel can ensure the control law of UAV heading angle change, as shown in Eq. (12).

$$\psi(t) = \psi_c \cdot (1 - e^{-\mu t}) \tag{12}$$

In Eq. (12), $\psi(t)$ represents the step response at zero state. ψ_c represents the heading command angle of the UAV. μ represents the time constant of the UAV heading channel model. Due to the fact that the UAV maintains its heading unchanged after converting to ψ_c, $\psi(t)$ can only complete the UAV's entry phase. However, throughout the entire conversion process, the UAV transitions from a CP to another CP, so the CP after entry can be regarded as obtained through symmetry before entry. Therefore, the heading angle change control law of the CD segment path in Fig. 4 can be obtained from the $\psi(t)$ of the entry segment AB. The waypoints at time t in the AB and CD segments are displayed in Eq. (13).

$$P_l(t) = P_l(t-1) + (v\Delta t \sin[\psi(t)], v\Delta t \cos[\psi(t)]) \tag{13}$$

In Eq. (13), $P_l(t)$ represents the waypoints of segment AB and CD at time t, and at time $t = 0$, the starting point of the path is $P_l(0) = (0,0)$, located at the origin of the coordinate system. The ACS-FP-CTPPA algorithm is Fig. 5.

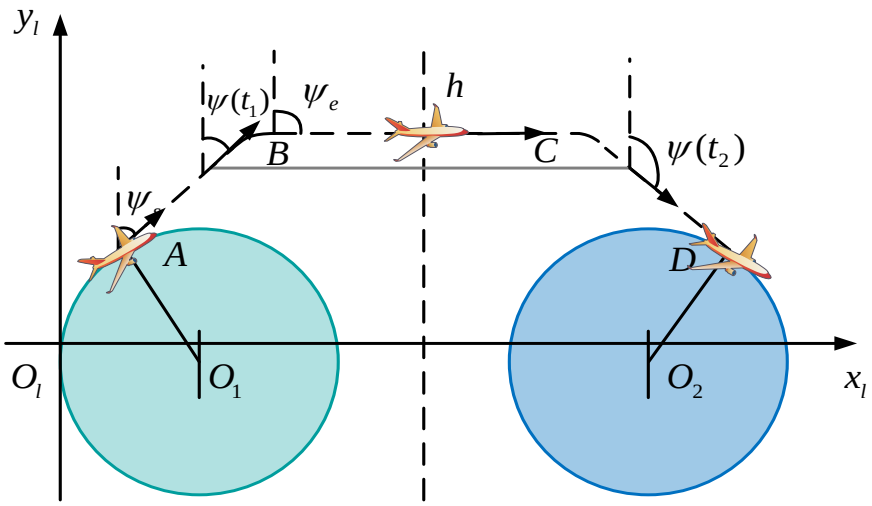

Fig. 4. Schematic diagram of path planning for switching between CPs.

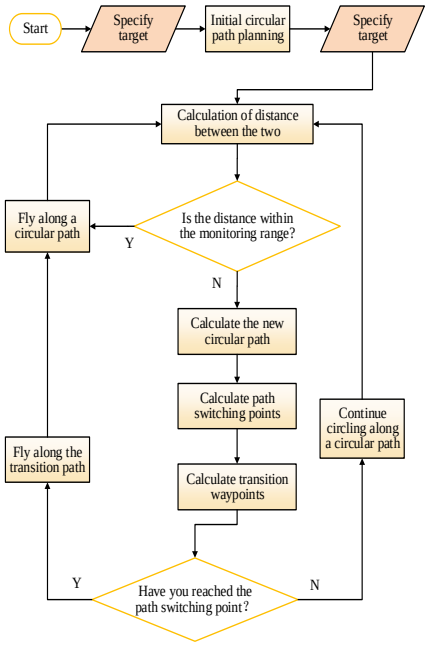

Fig. 5. Process of ACS-FP-CTPPA algorithm.

In Fig. 5, the first step is to determine the tracking target and perform initial CP planning on the target. Comparing whether the RD B-UAV/TT meets the conditions for real-time monitoring and illumination. If it meets the requirements, fly along the planned path. Otherwise, to calculate a new CP. Before switching to a new path, it is necessary to calculate the appropriate path-switching point and the position of the transition section waypoint. After reaching the switching point, to fly along the transition section path and switch to the next CP to continue flying. Repeating the path planning as the motion changes, otherwise continue flying along a CP and calculating the distance B-UAV/TT until the path switch is completed.

IV. Results and Discussion

This study compares the performance of ACS-FP-CTPPA with two commonly used pre-path planning algorithms, namely Turning Sensitive Ant Colony Optimization (TSACO) and Deep Q-network (DQN), by building a simulation experimental platform. Then, it is compared with Model Predictive Control Based on CTPPA (MPC-CTPPA) through outdoor real machine experiments to analyze the actual application effects.

A. Performance Testing of ACS-FP-CTPPA

To verify the feasibility of ACS-FP-CTPPA, this study used a computer with Windows 10 operating system and Intel (R) Core (TM) i5-9400F CPU, and built an experimental environment using UAVDT as the dataset. The number of iterations was set to 100. The comparison of convergence performance between ACS-FP-CTPPA, TSACO, and DQN algorithms in Fig. 6.

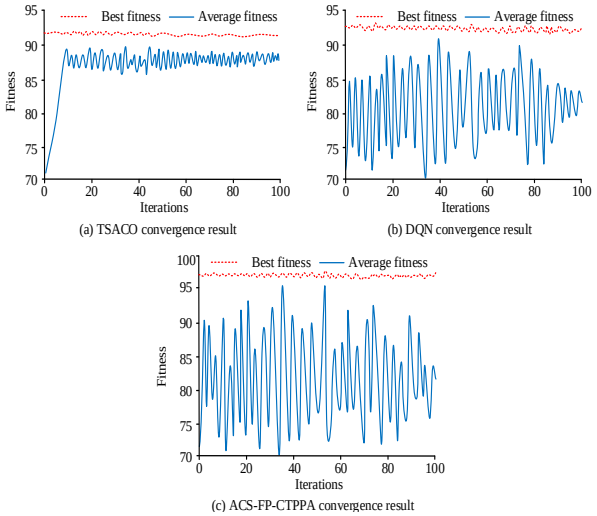

Fig. 6. Convergence performance of three algorithms on datasets.

In Fig. 6, (a), (b), and (c) show the convergence results of TSACO, DQN, and ACS-FP-CTPPA on the UAVDT dataset, respectively. The optimal fitness value for ACS-FP-CTPPA is 97.56, DQN is 93.87, and TSACO is 92.79. In order to verify the performance of different algorithms on different data sets, the study added DTB70 data set and UAV123 data set comparison test. The results of root mean square error (RSME), mean absolute percentage error (MAPE) and coefficient of determination are shown in Table II.

In Table II, due to the small number of sequences in the UAVDT dataset and the DTB70 dataset, the RSME and MAPE of the three algorithms on these two datasets are larger. In the DTB70 and UAV123 datasets, the RSME and MAPE of ACS-FP-CTPPA are significantly smaller than the other two comparison algorithms, indicating that the algorithm has the highest prediction accuracy in these two datasets. However, in the UAVDT data set, the RSME and MAPE of the three comparison algorithms are relatively close, which may lead to large error deviation due to the over-fitting phenomenon in the data set sequence. The values of ACS-FP-CTPPA on the three datasets are 0.9894, 0.9883 and 0.9987, respectively, which are larger than the other two algorithms and are closest to 1, indicating that the algorithm has the highest fitting degree. In the simulation experiment, for the convenience of observing data, both the UAV and the target are projected on the same horizontal plane, and the observation angle change maps under three planning algorithms are obtained as shown in Fig. 7.

In Fig. 7, the monitoring angle distribution range for targets under the TSACO algorithm is between -200° and 200°, under the DQN algorithm it is between -100° and 100°, and under the ACS-FP-CTPPA it is between 0° and 100°. This indicates that ACS-FP-CTPPA can provide a relatively stable irradiation time window and angle, while the other two comparison algorithms have a larger azimuth distribution range and cannot effectively provide a stable laser irradiation time window. Fig. 8 shows the trajectory and velocity curve of UAV movement.

Fig. 8(a) shows a comparison of UAV trajectories based on three algorithms, with TSACO planning having the longest total path and larger corner amplitudes. The total path planned by DQN is relatively short and there are corners. The total path planned by ACS-FP-CTPPA is the shortest and almost has no corners. Fig. 8(b) shows a comparison of UAV speeds among three algorithms. TSACO takes 49s with an average speed of 1.8m/s, making it the longest and slowest algorithm. DQN takes 46s, with an average speed of 2.6 m/s. ACS-FP-CTPPA takes 38s, with an average speed of 3.4m/s. This algorithm has the shortest time and the fastest average speed. Table III shows the results of three algorithms running on the Zakharov and Griewank functions.

TABLE II. COMPARISON OF ERRORS OF DIFFERENT ALGORITHMS ON DATASETS

Algorithm	Data set	RMSE	MAPE	R^2
TSACO	UAVDT	11.7678	7.7823	0.9764
	DTB70	14.9685	8.6452	0.9648
	UAV123	11.1325	7.5432	0.9750
DQN	UAVDT	11.9846	7.4637	0.9768
	DTB70	13.6516	8.3542	0.9730
	UAV123	10.6544	6.9841	0.9846
ACS-FP-CTPPA	UAVDT	11.6544	7.3135	0.9894
	DTB70	10.6844	7.1332	0.9883
	UAV123	8.2678	5.6451	0.9987

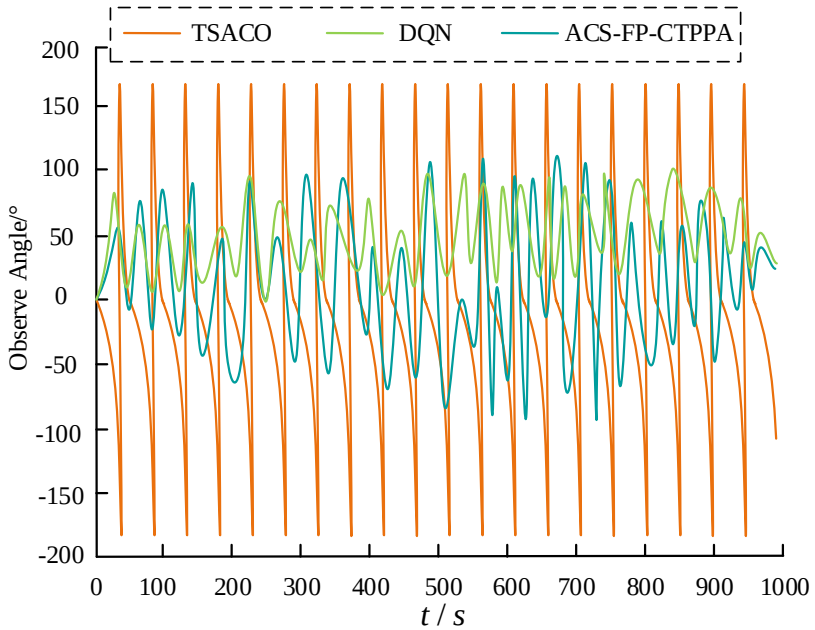

Fig. 7. Comparison chart of observation angle changes.

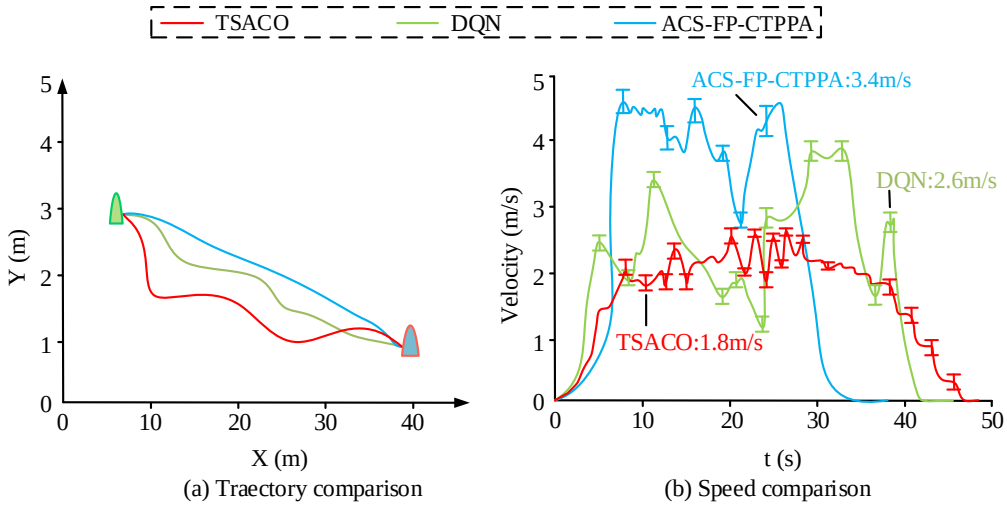

(a) Traectory comparison (b) Speed comparison

Fig. 8. The trajectory and velocity curve of UAV movement.

Table III shows the average, standard deviation, and optimal values of three algorithms tested on two sets of functions. ACS-FP-CTPPA has the lowest mean, standard deviation, and optimal value on both sets of functions, indicating that ACS-FP-CTPPA has better convergence accuracy and more stable calculation results.

B. *Application Analysis of UAV-T3P Based on ACS-FP-CTPPA*

To verify the feasibility of the designed PPA, ACS-FP-CTPPA and MPC-CTPPA are applied in real machine experiments to compare the actual application effects of the algorithm. The RealSense D435i camera provides an information source for environmental perception and conducts autonomous flight experiments in outdoor scenes. Fig. 9 shows the action trajectory of the UAV and target.

Fig. 9(a) shows the motion trajectory of UAV and target under ACS-FP-CTPPA. Six CPs and five transfer paths are planned along the entire path, with the UAV hovering on one side of the target. Fig. 9(b) shows the UVA and target path planned using MPC-CTPPA. During the flight, 16 CPs and 16 transfer paths are planned, and UAVs appear on various sides of the target. In contrast, the UAV tracking path planned by ACS-FP-CTPPA is more stable, and maintaining a certain RD during the tracking process is also a criterion for evaluating the quality of the path. Fig. 10 shows the RD between UAV and target in two algorithms for path planning.

TABLE III. QUANTITATIVE ANALYSIS RESULTS OF THREE ALGORITHMS

Function	Index	TSACO	DQN	ACS-FP-CTPPA
Zakharov	Mean	4.54e-24	9.50e-04	3.23e-71
	Standard deviation	5.21e-37	6.01e-02	4.02e-71
	Best	3.88e+01	4.01e+01	2.58e+01
Griewank	Mean	3.10e+02	5.30e+01	1.59e+02
	Standard deviation	5.46e+01	5.59e+01	3.66e+01
	Best	8.28e+04	2.19e-16	1.16e+01

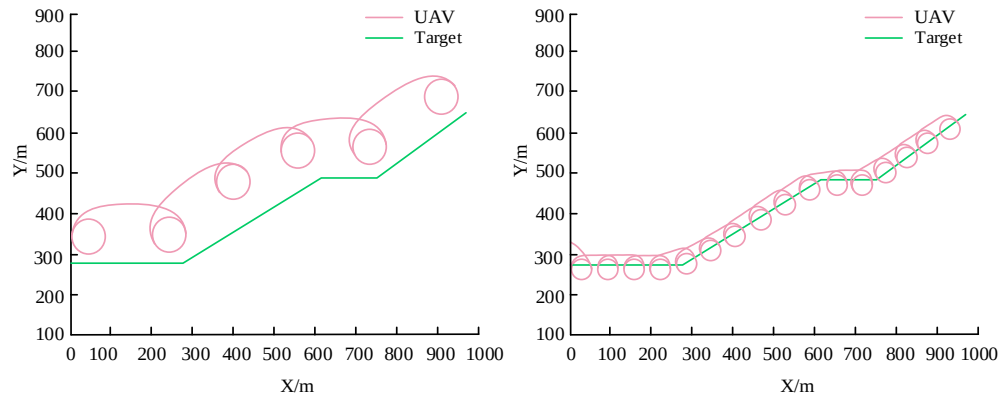

(a) ACS-FP-CTPPA planning algorithm path diagram (b) MPC-CTPPA planning algorithm path diagram

Fig. 9. Action trajectories of UAVs and targets under different algorithms.

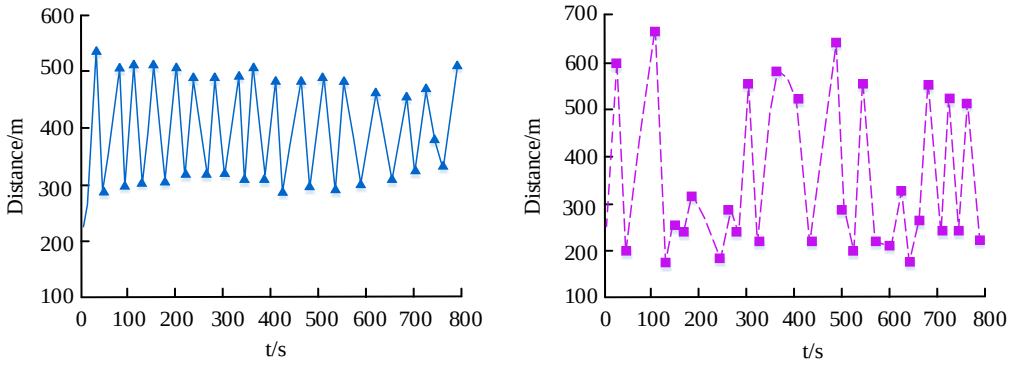

(a) Changes in relative distance between UAV and target under ACS-FP-CTPPA

(b) Changes in relative distance between UAV and target under MPC-CTPPA

Fig. 10. Changes in RD between UAV and target under different algorithms.

In Fig. 10(a), the curve fluctuates relatively uniformly up and down within the range of [200m, 600m], indicating a stable change in the RD between the UAV and the target. The curve in Fig. 10(b) fluctuates irregularly within [100m, 700m], and the RD between the UAV and the target is more unstable when it is close and far away. Compared with MPC-CTPPA, the UAV motion path planned by ACS-FP-CTPPA can maintain a more stable distance from the target, meeting the distance requirements for monitoring and illumination during flight missions. Finally, the correlation between the UAV tracking routes planned by different models and the actual flight routes is compared, as exhibited in Fig. 11.

In Fig. 11(a), the path planned by ACS-FP-CTPPA almost completely coincides with the actual flight path of the UAV. The path planned by MPC-CTPPA in Fig. 11(b) does not overlap with the actual path. This indicates that in practical applications, the UAV-T3P planned by ACS-FP-CTPPA can better achieve tracking tasks of photography and laser irradiation during flight, and has superior tracking effects.

(a) Comparison between Actual Trajectory and Planned Trajectory of ACS-FP-CTPPA

(b) Comparison between Actual Trajectory and Planned Trajectory of MPC-CTPPA

Fig. 11. Comparison of UVA actual trajectory and planned trajectory.

C. Discussion

UAVs are unable to autonomously plan suitable tracking paths based on changes in target motion during the process of tracking target detection. In view of this, this study digitized the motion relationship between UVA and tracking targets, and based on this, established ACS-CTPPA to calculate the center of a circular tracking path. Finally, the combination of ACS-CTPPA and UAV tracking photography resulted in a highly adaptive ACS-FP-CTPPA algorithm. In the performance test of simulation experiments, the best fitness of ACS-FP-CTPPA, DQN and TSACO algorithms are 97.56,93.87 and 92.79, respectively. The best fitness of ACS-FP-CTPPA is significantly higher than that of DQN and TSACO. The convergence performance is significantly better than the convergence speed of the control model proposed by Saeed R A et al.in literature [17]. The error results on three different datasets show that ACS-FP-CTPPA is 0.9894, 0.9883 and 0.9987, respectively, which is significantly larger than the other two comparison algorithms and is closest to 1, indicating that the algorithm has the best fitting performance. At the same time, in the DTB70 and UAV123 datasets, the RSME and MAPE values of ACS-FP-CTPPA are the smallest among the three algorithms, showing higher prediction accuracy, which is better than the prediction performance of the algorithm proposed by Cao Y et al. [18]. The monitoring angle distribution range for targets under TSACO and DQN algorithms was within [-200°, 200°] and [-100°, 100°], respectively. The monitoring angles for targets under the ACS-FP-CTPPA algorithm were distributed at [0°, 100°]. Under the tracking path planned by ACS-FP-CTPPA, the UAV's illumination angle remained stable during flight. The comparison of UAV motion trajectories under three algorithms showed that the total path planned by ACS-FP-CTPPA was the shortest and took the shortest 38s, with an average speed of 3.4m/s.

In summary, the ACS-FP-CTPPA algorithm proposed in this study shows excellent performance in both simulation experiments and practical applications. It is superior to the existing DQN and TSACO algorithms in terms of fitness,

monitoring angle stability, path planning efficiency and relative distance stability. Although there are some limitations, through further research and optimization, the ACS-FP-CTPPA algorithm is expected to play a greater role in future UAV tracking tasks.

V. Conclusion

In order to optimize the path planning control performance of UAV in tracking target, the model is constructed by combining the motion model of UAV and the adaptive control circular tracking path planning algorithm. The results show that the UAV circular path under ACS-FP-CTPPA planning is 6, and the path switching process under ACS-FP-CTPPA is less, indicating that the algorithm has better path planning performance. Under the ACS-FP-CTPPA algorithm, the relative distance curve between UAV and target fluctuates relatively evenly in the range of [200m, 600m], while the relative distance curve of MPC-CTPPA fluctuates irregularly in the range of [100m, 700m]. The comparison results show that the ACS-FP-CTPPA algorithm has significant advantages in maintaining the stability of the relative distance between the UAV and the target, which further proves the feasibility and effectiveness of the algorithm. However, the research is to map the entire UAV tracking process to a two-dimensional plane coordinate for analysis, ignoring factors that may affect the model such as the dynamic level. Subsequent research can conduct in-depth research on this aspect.

References

[1] Yuan D, Chang X, Li Z, Li Z, He Z. Learning adaptive spatial-temporal context-aware correlation filters for UAV tracking. ACM Transactions on Multimedia Computing, Communications, and Applications (TOMM), 2022, 18(3): 1-18.

[2] Apostolidis S D, Kapoutsis P C, Kapoutsis A C, Kosmatopoulos E B. Cooperative multi-UAV coverage mission planning platform for remote sensing applications. Autonomous Robots, 2022, 46(2): 373-400.

[3] Daud S M S M, Yusof M Y P M, Heo C C, Khoo L S, Singh M K C, Mahmood M S, Nawawi H. Applications of drone in disaster management: A score review. Science & Justice, 2022, 62(1): 30-42.

[4] Jackman A. Visualizations of the small military drone: Normalization through ‘naturalization’. Critical Military Studies, 2022, 8(4): 339-364.

[5] Puente-Castro A, Rivero D, Pazos A, Fernandez-Blanco E. A review of artificial intelligence applied to path planning in UAV swarms. Neural Computing and Applications, 2022, 34(1): 153-170.

[6] Jones M, Djahel S, Welsh K. Path-planning for unmanned aerial vehicles with environment complexity considerations: A survey. ACM Computing Surveys, 2023, 55(11): 1-39.

[7] Adekola O D, Udekwu O K, Saliu O T, et al. Object Tracking-Based" Follow-Me" Unmanned Aerial Vehicle (UAV) System. Comput. Syst. Sci. Eng., 2022, 41(3): 875-890.

[8] Saminu S, Xu G, Zhang S, Kader IAE, Aliyu HA, Jabire AH, Ahmed YK, Adamu MJ. Applications of Artificial Intelligence in Automatic Detection of Epileptic Seizures Using EEG Signals: A Review. Artificial Intelligence and Applications, 2023,1(1): 11-25.

[9] Xiao M, Liang J, Ji L, Sun Z, Li Z Y. Aerial photography trajectory-tracking controller design for quadrotor UAV. Measurement and Control, 2022, 55(8): 738-745.

[10] Bottrell C, Hani M H, Teimoorinia H, Patton D R, Ellison S L. The combined and respective roles of imaging and stellar kinematics in identifying galaxy merger remnants. Monthly Notices of the Royal Astronomical Society, 2022, 511(1): 100-119.

[11] Li J, Sun Y, Li X, Xie S, Lin J, Su M. Observer-based adaptive control for single-phase UPS inverter under nonlinear load. IEEE Transactions on Transportation Electrification, 2022, 8(2): 2785-2796.

[12] Pang N, Wang X, Wang Z. Event-triggered adaptive control of nonlinear systems with dynamic uncertainties: The switching threshold case. IEEE Transactions on Circuits and Systems II: Express Briefs, 2022, 69(8): 3540-3544.

[13] Yang Y, Ye X, Wen B, Huang J, Su X. Adaptive control design for uncertain underactuated cranes with nonsmooth input nonlinearities. IEEE Transactions on Systems, Man, and Cybernetics: Systems, 2022, 53(2): 1074-1083.

[14] O’Hagan L A, Serafinelli E. Transhistoricizing the drone: A comparative visual social semiotic analysis of pigeon and domestic drone photography. Photography and Culture, 2022, 15(4): 327-351.

[15] Wong Y W A, Ernesto P, Elias J. Comparative study of aerial photography/(UAV)-drone vs 16th century cityscape art. IDA: International Design and Art Journal, 2022, 4(1): 57-75.

[16] Serafinelli E, O’Hagan L A. Drone views: a multimodal ethnographic perspective. Visual Communication, 2024, 23(2): 223-243.

[17] Saeed R A, Omri M, Abdel-Khalek S, Ali E , Alotaibi M F. Optimal path planning for drones based on swarm intelligence algorithm. Neural Computing and Applications, 2022, 34(12): 10133-10155.

[18] Cao Y, Cheng X, Mu J. Concentrated coverage path planning algorithm of UAV formation for aerial photography. IEEE Sensors Journal, 2022, 22(11): 11098-11111.

[19] Shen K, Shivgan R, Medina J, Dong Z, Rojas-Cessa R. Multidepot drone path planning with collision avoidance. IEEE Internet of Things Journal, 2022, 9(17): 16297-16307.

[20] Puente-Castro A, Rivero D, Pazos A, Fernandez-Blanco E. UAV swarm path planning with reinforcement learning for field prospecting. Applied Intelligence, 2022, 52(12): 14101-14118.